DOI: 10.13009/EUCASS2025-377
11TH EUROPEAN CONFERENCE FOR AERONAUTICS AND SPACE SCIENCES (EUCASS)

ZND MODELING OF A DETONATION IN A TWO-PHASE KEROSENE-AIR MIXTURE

Emrys BOUISSON [1], *Dmitry DAVIDENKO* [1], *Thomas GAILLARD* [1], *Joël DUPAYS* [1] *and Wei Long SIAUW* [2]

[1]*Department of Multi-Physics for Energetics, ONERA, Paris-Saclay University, 91123 Palaiseau, France*
[2]*DSO National Laboratories, 11 Stockport Road, Singapore 117605*
emrys.bouisson@onera.fr, www.onera.fr

Abstract

This paper presents Zel'dovich-von Neumann-Döring (ZND) modeling of a detonation in a two-phase kerosene-air mixture. An Eulerian-Eulerian system of ordinary differential equations is developed. Influence of momentum, thermal, and mass exchanges in a non-reacting flow is studied first. A case of reacting flow in a CJ detonation is analyzed in detail considering profiles of flow parameters and thermicity terms. A parametric study of CJ detonation is performed by varying the droplet diameter and the mass ratio of liquid fuel. Different characteristic lengths are analyzed to highlight the effect of these parameters on the principle processes in a detonation wave.

Nomenclature

Greek symbols

α	Volume fraction
β	Liquid mass fraction
λ	Thermal conductivity
μ	Dynamic viscosity
Ψ	Droplet property breakup rate
ρ	Density
σ	Thermicity

Latin symbols

$\dot{m}$	Mass exchange rate
$\mathcal{D}$	Diffusion coefficient
$\mathcal{E}$	Total energy
$\mathcal{M}$	Molar mass
a	Sound speed
C_d	Drag coefficient
c_p	Specific heat
D	Diameter
f_p	Drag force
G, F, E	Source terms
h	Enthalpy
l	Characteristic length
L_{vap}	Latent heat of vaporization
Le	Lewis number
M	Mach number
m	Mass
n	Droplet number density
Nu	Nusselt number
P	Pressure
Pr	Prandtl number
Q_p	Thermal exchange rate
Re	Reynolds number
Sc	Schmidt number
Sh	Sherwood number
T	Temperature
u	Velocity in laboratory reference frame
V	Velocity in detonation reference frame
x, X	Distance from shock front
Y	Mass fraction

Subscript

0	Initial conditions
d	Droplet
e	Evaporation
F	Evaporating fuel
$F_{0.5}$	50% of fuel consumed
$F_{0.95}$	95% of fuel consumed
g	Gas phase
k	Species index
p	Dispersed phase
$surf$	Surface
T	Temperature
v	Velocity

Superscript

ch	Chemical process
vap	Vaporization process

DOI: 10.13009/EUCASS2025-377

1. Introduction

Propulsion using detonation combustion can offer a significant gain in engine performance due to its increased thermodynamic efficiency in comparison with the conventional Bryton cycle. The rotating detonation engine (RDE) has particular advantages due to continuous detonation propagation in an annular chamber. It can be considered for air-breathing applications as a turbojet, for which the use of a liquid hydrocarbon fuel is of practical interest. Recent experimental and numerical studies[1,2] have shown the feasibility of RDE operation with liquid kerosene.

Obtaining a stably propagating detonation in a mixture of liquid kerosene and air presents certain challenges. Both the chemical nature and liquid state of the hydrocarbon fuel narrow stability conditions for a detonation. Before the combustion can start, fuel droplets need to be heated and vaporized to produce a reactive fuel-air mixture. Kerosene is composed of heavy hydrocarbon molecules, for which the reaction time is long, compared to light molecules such as hydrogen. Both factors make the reaction zone behind a leading shock rather long and prone to perturbations, which can affect the detonation wave stability. Other factors can also be considered, such as the droplet breakup process when the droplets cross the shock wave, especially when the speed difference and droplet size are important.[3,4] The two-phase and chemical kinetic processes need be studied in detail to understand their mutual roles in a detonation wave.

The classical Zel'dovich-von Neumann-Döring (ZND) model permits the description of the flow structure behind a shock for a gaseous kerosene-air mixture, and the Chapman-Jouguet (CJ) theory shows good predictions for the propagation velocity with respect to experimental data. This model cannot describe a detonation in a two-phase mixture. Several studies have developed a similar type of model considering a two-phase mixture with a granular material in Powers et al.,[5,6] with solid particles in Zhang et al.[7] and Zhou et al.,[8] and also with liquid particles in Martínez-Ruiz.[9]

This paper presents a numerical study using a ZND-type model for a detonation wave in a two-phase kerosene-air mixture, in a similar way to Martínez-Ruiz,[9] with chemical kinetics, represented by a global reaction mechanism, and a physical model adapted for high-Reynolds number, compressibility, and evaporation film effects. Firstly, a ZND model, is formulated for a one-dimensional steady-state two-phase reacting flow behind a normal shock. The resulting system of ODE, derived from the Euler equations for the compressible gas and dispersed phase,[10] is integrated by a high-order method with an adaptive spatial step. A two-way coupling between the phases is set up by introducing source terms for the drag force, heat and mass exchanges. Secondly, a study of several physical factors is presented for inert and reacting two-phase flows behind a shock. And thirdly, a parametric study is done to highlight the effect of initial conditions (droplet diameter and pre-evaporation factor) on the reaction zone structure in a CJ detonation wave.

2. ZND Model

2.1 Governing equations

An Eulerian-Eulerian formulation is chosen to describe the evolution of a two-phase system behind a shock in a 1D approach. It is supposed that the liquid phase is represented by monodispersed droplets. A system of four governing equations is formulated for each phase. The gas phase is described by equations (1) to (4) and the liquid phase by (5) to (8). Source terms are added to couple these systems: G for mass exchange (9), F for momentum exchange (10), and E for energy exchange (11).

$$\frac{\partial}{\partial t}(\alpha_g \rho_g) + \frac{\partial}{\partial x}(\alpha_g \rho_g u_g) = G \tag{1}$$

$$\frac{\partial}{\partial t}(\alpha_g \rho_g u_g) + \frac{\partial}{\partial x}(\alpha_g \rho_g u_g^2 + \alpha_g P_g) = F \tag{2}$$

$$\frac{\partial}{\partial t}(\alpha_g \rho_g \mathcal{E}_g) + \frac{\partial}{\partial x}\left(\alpha_g \rho_g u_g \left(h_g + u_g^2/2\right)\right) = E \tag{3}$$

$$\frac{\partial}{\partial t}(\alpha_g \rho_g Y_k) + \frac{\partial}{\partial x}(\alpha_g \rho_g u_g Y_k) = \dot{m}_k^{vap} + \dot{m}_k^{ch} \tag{4}$$

$$\frac{\partial}{\partial t}(\alpha_p \rho_d) + \frac{\partial}{\partial x}(\alpha_p \rho_d u_p) = -G \tag{5}$$

$$\frac{\partial}{\partial t}(\alpha_p \rho_d u_p) + \frac{\partial}{\partial x}(\alpha_p \rho_d u_p^2 + \alpha_p P_p) = -F \tag{6}$$

$$\frac{\partial}{\partial t}(\alpha_p \rho_d \mathcal{E}_p) + \frac{\partial}{\partial x}\left(\alpha_p \rho_d u_p \left(h_p + u_p^2/2\right)\right) = -E \tag{7}$$

$$\frac{\partial}{\partial t}(n_p) + \frac{\partial}{\partial x}(n_p u_p) = \Psi_p \tag{8}$$

DOI: 10.13009/EUCASS2025-377

$$G = \dot{m}^{vap} \tag{9}$$
$$F = u_p \dot{m}^{vap} - f_p \tag{10}$$
$$E = \left(h_p + u_p^2/2\right) \dot{m}^{vap} - u_p f_p - Q_p \tag{11}$$

Some hypotheses are made regarding these equations. Firstly, the reference frame is changed from the laboratory to the detonation wave to consider a steady-state flow. So the velocity is introduced as $V = D - u$ where D is the shock velocity. Secondly, the volume fraction of the liquid phase is negligible compared to the gas phase, and the liquid is considered incompressible, therefore $\alpha_g = 1$ and $P_p = 0$. Thirdly, the perfect-gas equation is used for the gas state. Lastly, the break-up process is not considered in this study by setting $\Psi_p = 0$. By introducing the mass concentration of droplets as $\rho_p = \alpha_p \rho_d$, with $\alpha_p = \frac{\pi}{6} D_p^3 n_p$, the simplified equations are :

$$\frac{\partial}{\partial x}(\rho_g V_g) = G \tag{12}$$
$$\frac{\partial}{\partial x}(\rho_g V_g^2 + P_g) = F \tag{13}$$
$$\frac{\partial}{\partial x}\left[\rho_g V_g \left(h_g + V^2/2\right)\right] = E \tag{14}$$
$$\frac{\partial}{\partial x}(\rho_g V_g Y_k) = \dot{m}_k^{vap} + \dot{m}_k^{ch} \tag{15}$$
$$\frac{\partial}{\partial x}(\rho_p V_p) = -G \tag{16}$$
$$\frac{\partial}{\partial x}(\rho_p V_p^2) = -F \tag{17}$$
$$\frac{\partial}{\partial x}\left[\rho_p V_p \left(h_p + V^2/2\right)\right] = -E \tag{18}$$
$$\frac{\partial}{\partial x}(n_p V_p) = 0 \tag{19}$$

In the same way as in the classical ZND model, equations (12) to (19) can be rewritten into ordinary differential equations to be integrated. Equations (20) to (27) form the final equations system. Variable σ, called global thermicity, is composed of five elements (28). The first three correspond to the mass exchange, σ_1 (29), momentum exchange, σ_2 (30), and energy exchange, σ_3 (31). The last two are due to the change in species mass fraction by chemical reactions, σ_4 (32), and evaporation, σ_5 (33).

Note that the classical ZND model can be found from equations (20) to (23) if all source terms, excepting the chemical ones, are set equal to zero. In this case, the global thermicity will only contain σ_4.

$$\frac{\partial V_g}{\partial x} = \frac{\sigma}{1 - M^2} \tag{20}$$
$$\frac{\partial \rho_g}{\partial x} = \frac{G}{V_g} - \frac{\rho_g}{V_g} \frac{\sigma}{1 - M^2} \tag{21}$$
$$\frac{\partial P_g}{\partial x} = -G V_g + F - \rho_g V_g \frac{\sigma}{1 - M^2} \tag{22}$$
$$\frac{\partial Y_k}{\partial x} = \frac{\dot{m}_k^{vap} - Y_k G + \dot{m}_k^{ch}}{\rho_g V_g} \tag{23}$$
$$\frac{\partial V_p}{\partial x} = -\frac{F}{\rho_p V_p} + \frac{G}{\rho_p} \tag{24}$$
$$\frac{\partial \rho_p}{\partial x} = -\frac{G}{V_p} - \frac{\rho_p}{V_p} \frac{\partial V_p}{\partial x} \tag{25}$$
$$\frac{\partial h_p}{\partial x} = \frac{-E + V_p F + G\left(h_p - V_p^2/2\right)}{\rho_p V_p} \tag{26}$$
$$\frac{\partial n_p}{\partial x} = -\frac{n_p}{V_p} \frac{\partial V_p}{\partial x} \tag{27}$$

DOI: 10.13009/EUCASS2025-377

$$\sigma = \sigma_1 + \sigma_2 + \sigma_3 + \sigma_4 + \sigma_5 \tag{28}$$

$$\sigma_1 = \frac{1}{\rho_g} G \tag{29}$$

$$\sigma_2 = \frac{V_g}{P_g}(V_g G - F) \tag{30}$$

$$\sigma_3 = \frac{1}{\rho_g c_p T_g}\left[E - \left(h + V_g^2/2\right) G\right] \tag{31}$$

$$\sigma_4 = \frac{1}{\rho_g}\sum_{k=1}^{n}\left(\frac{\mathcal{M}}{\mathcal{M}_k} - \frac{h_k}{c_p T_g}\right)\dot{m}_k^{ch} \tag{32}$$

$$\sigma_5 = \frac{1}{\rho_g}\sum_{k=1}^{n}\left(\frac{\mathcal{M}}{\mathcal{M}_k} - \frac{h_k}{c_p T_g}\right)(\dot{m}_k^{vap} - Y_k G) \tag{33}$$

2.2 Chemical kinetic model

The chemical kinetic model for the JP-10, considered as fuel in the present study, is inspired by the reduced model from Varatharajan et al.[11] The used model consists of a global step of JP-10 oxidation and 5 elementary reactions for the H-O system and CO conversion into CO_2, given in table 1. The Cantera library (https://cantera.org/) is used, to calculate the production rates for the gaseous species as well as for the thermodynamic and molecular transport properties of the gas mixture.

Table 1: Six-step semi-global mechanism for JP-10

$C_{10}H_{16} + 9\,O_2 \longrightarrow 10\,CO + \frac{19}{3}H_2O + \frac{5}{3}H + \frac{5}{3}OH$
$H + O_2 \longleftrightarrow OH + O$
$H_2 + O \longleftrightarrow OH + H$
$H_2 + OH \longleftrightarrow H_2O + H$
$H + OH + M \longleftrightarrow H_2O + M$
$CO + OH \longleftrightarrow CO_2 + H$

2.3 Drag force model

The drag force is expressed by the following equation equation:

$$f_p = n_p \frac{\pi}{8} Re_p \mu_g D_p C_d (V_g - V_p) \tag{34}$$

Several models can be chosen to determine the drag coefficient, C_d: a simple one as the model of Schiller and Naumann[12] or more complex for compressible flow as the model of Henderson[13] or the more recent one by Loth.[14] The latter is used for the results of this paper. The formulation of the drag coefficient for continuum flows, with $Re_p \geqslant 45$, is described by equations (35) to (38). This model is built upon a modified Clift-Gauvin drag law (35) where an empirical correction of Mach number effect is applied (37) and empirical relations ((36) and (38)) are used to reduce the compressibility effect as the Reynolds number decreases. The particle Mach number, $M_p = \frac{|V_g - V_p|}{a_g}$, is the key parameter that defines compressibility.

$$C_d = \frac{24}{Re_p}(1 + 0.15 Re_p^{0.687}) H_M + \frac{0.42 C_M}{1 + \frac{42500 G_M}{Re_p^{1.16}}} \tag{35}$$

$$H_M = 1 - \frac{0.258 C_M}{1 + 514 G_M} \tag{36}$$

$$C_M = \begin{cases} \frac{5}{3} + \frac{2}{3}\tanh(3\ln(M_p + 0.1)) & \text{for } M_p \leq 1.45 \\ 2.044 + 0.2 e^{-1.8 \ln\left(\frac{M_p}{1.5}\right)^2} & \text{for } M_p > 1.45 \end{cases} \tag{37}$$

$$G_M = \begin{cases} 1 - 1.525 M_p^4 & \text{for } M_p \leq 0.89 \\ 10^{-4}\left(2 + 8\tanh\left(12.77\left(M_p - 2.02\right)\right)\right) & \text{for } M_p > 0.89 \end{cases} \tag{38}$$

DOI: 10.13009/EUCASS2025-377

2.4 Thermal exchange and evaporation models

In the case of non-evaporating droplets, equation (39) represents the thermal exchange rate between gas and droplets.

$$Q_p = n_p \pi D_p Nu \lambda (T_g - T_p) \tag{39}$$

The evaporation model of Abramzon and Sirignano[15] is implemented in the present ZND model. If evaporation occurs, the thermal exchange rate between gas and droplets is obtained by (40) and the mass exchange rate by (41). Note that $\overline{*}$ corresponds to an intermediate gas state between those far from the droplet and at the droplet surface, as defined in (42) and (43), where the weighting parameter k is taken equal to a recommended value[16] of 1/3 . This model considers the presence of a film around the droplet, which can significantly affect the amount of heat and mass exchange. The first step, to find the mass exchanges rate, consists in calculation of the Spalding mass transfer number (44), diffusional film correction factor (45), and modified Sherwood number (46). The second step, to find the thermal exchange rate, needs iterative calculation of the film correction factor (47), modified Sherwood number (46), Φ parameter (49), and Spalding thermal transfer number (50). The Lewis number is given by $\overline{Le_F} = \frac{\overline{\lambda_g}}{\overline{\rho_g}\,\overline{\mathcal{D}_F}\,\overline{c_{p,g}}}$.

$$Q_p = \dot{m}_F^{vap} \left(\frac{\overline{c_{p,F}}(T_g - T_p)}{B_T} - L_{vap}(T_p) \right) \tag{40}$$

$$\dot{m}_F^{vap} = n_p \pi d_p \overline{\rho_g}\,\overline{\mathcal{D}_F} Sh^* \ln(1 + B_M) \tag{41}$$

$$\overline{Y} = Y_{g,surf} + k(Y_g - Y_{g,surf}) \tag{42}$$

$$\overline{T} = T_p + k(T_g - T_p) \tag{43}$$

$$B_M = \frac{Y_{F,surf} - Y_F}{1 - Y_{F,surf}} \tag{44}$$

$$F(B_M) = (1 + B_M)^{0.7} \frac{\ln(1 + B_M)}{B_M} \tag{45}$$

$$Sh^* = 2 + \frac{Sh - 2}{F(B_M)} \tag{46}$$

$$F(B_T) = (1 + B_T)^{0.7} \frac{\ln(1 + B_T)}{B_T} \tag{47}$$

$$Nu^* = 2 + \frac{Nu - 2}{F(B_T)} \tag{48}$$

$$\Phi = \frac{\overline{c_{p,F}}}{\overline{c_{p,g}}} \frac{Sh^*}{Nu^*} \frac{1}{\overline{Le_F}} \tag{49}$$

$$B_T = (1 + B_M)^{\Phi} - 1 \tag{50}$$

$$\tag{51}$$

In the same way as the drag coefficient, the Nusselt and Sherwood numbers can be expressed in various ways. The model of Ranz and Marshall[17] does not include compressible effects, equations (52) and (53), whereas the model of Carlson and Hoglund[18] takes them into account. Both models give similar results but in this study, the first model is used due to numerical stability issues.

$$Nu = 2 + 0.6 \sqrt{Re_p} Pr^{1/3} \tag{52}$$

$$Sh = 2 + 0.6 \sqrt{Re_p} Sc^{1/3} \tag{53}$$

DOI: 10.13009/EUCASS2025-377

2.5 Characteristic lengths definition

In a two-phase detonation, different flow dynamics are present. In order to compare how the droplet diameter and liquid fraction impact the flow structure, some characteristic lengths are introduced. Three lengths characterize the interaction between the gas and liquid phases: the momentum exchange l_v, the thermal exchange l_T, and the droplet evaporation l_m. The first one is the distance from the leading shock to the station, where the droplet velocity is at 50% between the initial and final values. The second is the distance where the droplet temperature is at 50% between the initial and final temperatures, which is equilibrium temperature or final state definition in the case of evaporating droplet. The third is the distance where 50% of the droplets mass is vaporized. Two other lengths are considered, $l_{F_{0.5}}$ and $l_{F_{0.95}}$, which correspond respectively to the consumption of 50% and 95% of the total kerosene mass.

2.6 Computational code

The computational code, implementing the described ZND model, is written in Python. Integration of equations (20) to (27) is done with the Python library Scipy (https://scipy.org/). The method used for the ODE system integration is "LSODA", an implicit solver with adaptive step and error control from ODEPAC,[19] detailed in Petzold.[20]

The Python library SDtoolbox[21] is used to determine the post-shock gas state as well as the CJ speed for a gaseous mixture. For liquid phase, droplet initial parameters are considered unaffected by the shock. The CJ detonation speed in a two-phase mixture is determined iteratively by a shooting method: the wave velocity D is adjusted until the equilibrium state reaches the sonic condition.

3. Results

This part studies the flow structure behind a shock for different initial conditions. First, how each physical factor influences the flow behaviour. Then a parametric study of a CJ detonation is presented. As initial state, for all the cases, the pressure is 1 bar, the temperature is 350 K, and the global equivalence ratio is 1.

In sections 3.1 to 3.3, the initial state and post-shock parameters for both phases are specified in table 2. These values are obtained with 70% of the total kerosene mass in liquid phase. These parameters correspond to a CJ detonation described in section 3.4.

Table 2: Initial state and post-shock parameters with 70% of the total kerosene mass in liquid phase

Gas phase	Initial state	Post-shock
P_g (MPa)	0.1	2.781
T_g (K)	350	1670.7
ρ_g (kg/m^3)	1.008	5.871
V_g (m/s)	1791.8	307.6

Liquid phase	Initial and post-shock state
T_p (K)	350
V_p (m/s)	1791.8

3.1 Momentum exchange

First, only the drag factor is considered in a non-reacting flow with adiabatic, non evaporating droplets. In equations (9) to (11), $\dot{m}^{vap} = 0$ and $Q_p = 0$, and in (32) and (33), $\dot{m}_k^{ch} = 0$ and $\dot{m}_k^{vap} = 0$. Figure 1 shows flow parameter profiles for droplet diameters of 5 µm and 50 µm.

For both phases, the final equilibrium speed is slightly lower than the gas velocity right behind the shock. The higher droplet velocity does not increase the gas velocity by momentum exchange. However, this will result in gas compression with an overall increase in pressure, density, and temperature. Note that in the beginning, the droplet drag increases slightly the gas velocity, which is illustrated by the decrease in the gas density, but the Mach number is always decreasing due to the sound speed growth despite the small acceleration.

The droplet diameter has an effect on the delay of parameter variation but not on the profile shape. Indeed, the bigger the diameter, the longer it will take to reach the equilibrium state. Table 3 shows the characteristic length of momentum exchange. The length for the diameter of 50 µm is more than ten times larger than for 5 µm.

DOI: 10.13009/EUCASS2025-377

Table 3: Characteristic length for momentum exchange of adiabatic, non-evaporating droplets

	D_p = 5 µm	D_p = 50 µm
l_v (m)	1.099×10^{-3}	1.294×10^{-2}

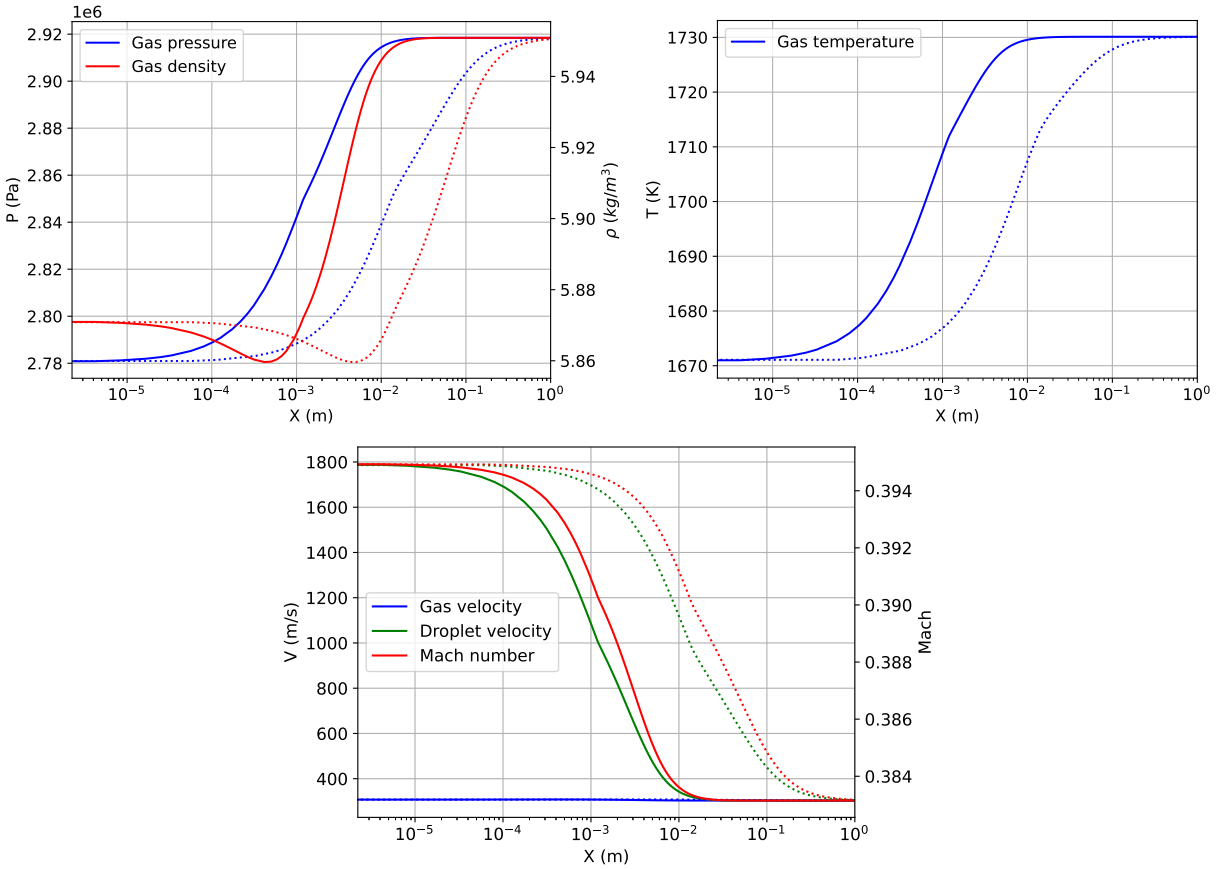

Figure 1: Parameter profiles versus post-shock distance for a non-reacting flow with adiabatic, non-evaporating droplets of 5 µm (solid lines) and 50 µm (dotted lines)

3.2 Thermal exchange

In addition to the drag, thermal exchange between gas and particles is now considered in a non-reacting flow with non-evaporating droplets. In equations (9) to (11), $\dot{m}^{vap} = 0$, and in (32) and (33), $\dot{m}_k^{ch} = 0$ and $\dot{m}_k^{vap} = 0$. Figure 2 shows flow parameter profiles for droplet diameters of 5 µm and 50 µm.

The velocity profiles are similar to those of the previous case (figure 1). However, due to thermal exchange, the overall variation of the velocity, pressure, and density is greater. The drag effect causes an initial rise in gas temperature, then, a decrease occurs during thermal exchange, while the droplet temperature increases until an equilibrium is reached. One can notice a slope brake on the droplet temperature curves at approximately 700 K. This is because temperature polynomials for the thermodynamic properties of the liquid kerosene are defined up to the critical point of 680 K, above which the vapor phase properties are used.

The droplet diameter has the same effect on the parameter behaviour as in the previous case. Table 4 shows the characteristic lengths of momentum and thermal exchange. The momentum length is similar compared to the case with drag only (table 3). The heat exchange is strongly delayed as the thermal length is larger by a factor of 5 for 5 µm and 18 for 50 µm.

DOI: 10.13009/EUCASS2025-377

Table 4: Characteristic lengths for momentum and thermal exchange for a non-reacting flow with non-evaporating droplets

	D_p = 5 µm	D_p = 50 µm
l_v (m)	1.142×10^{-3}	1.283×10^{-2}
l_T (m)	5.841×10^{-3}	2.310×10^{-1}

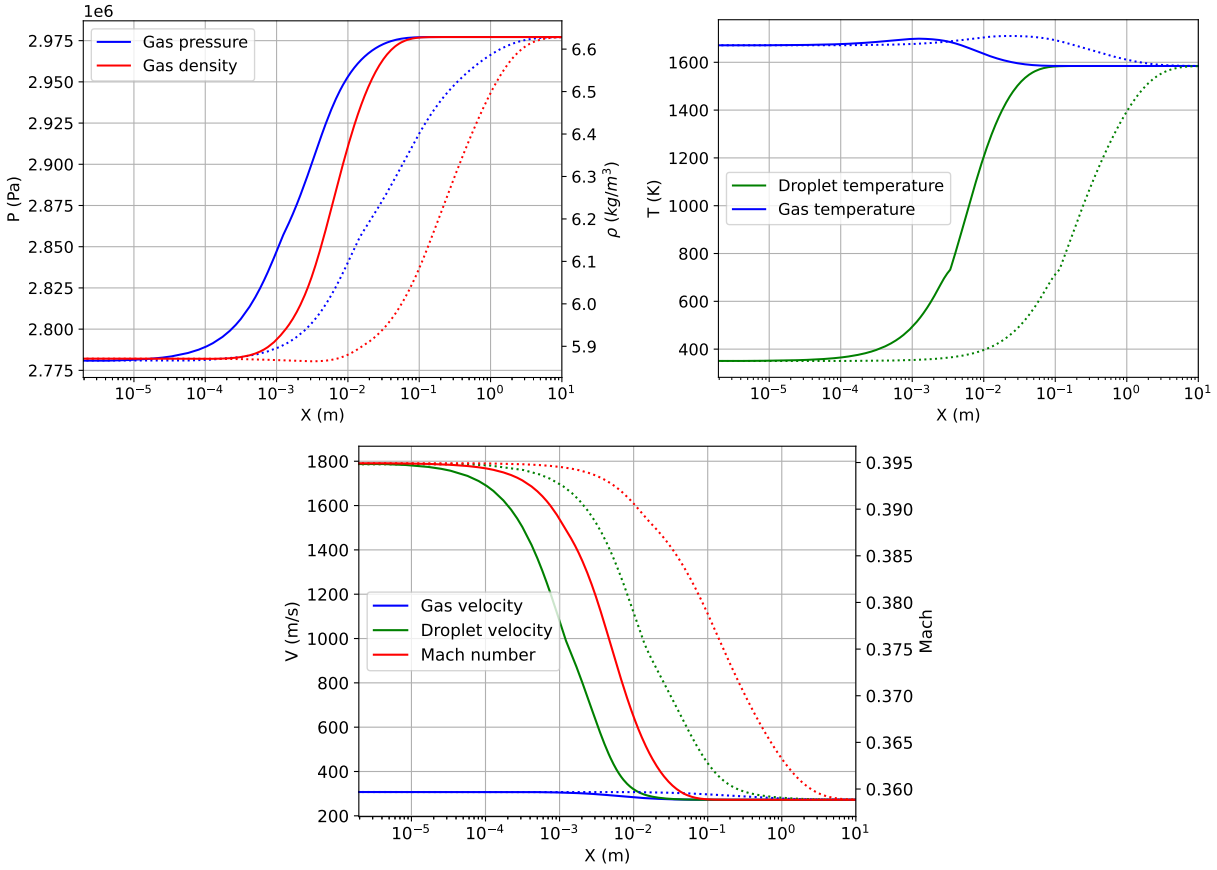

Figure 2: Parameter profiles versus post-shock distance for a non-reacting flow with non-evaporating droplets of 5 µm (solid lines) and 50 µm (dotted lines)

3.3 Mass exchange

Droplet evaporation is added to the momentum and heat exchanges. The flow is still non-reacting, $\dot{m}_k^{ch} = 0$ in equation (32). Figure 3 shows flow parameter profiles for droplet diameters of 5 µm and 50 µm.

The overall parameter variations are almost identical to those in the preceding case involving thermal exchange (figure 2), excepting the droplet temperature. The profile shapes remain similar while the droplet mass stays unchanged. Droplet evaporation causes changes in parameter profile slopes and strongly limits the increase in droplet temperature.

Table 5 presents characteristic lengths of momentum, thermal, and mass exchanges. These data indicate an accelerated transition to equilibrium thanks to evaporation. Due to the smaller change in droplet temperature, the characteristic thermal length is strongly reduced as compared to the previous case without evaporation (table 4). The characteristic length of mass exchange is much larger because the evaporation rate depends strongly on the droplet temperature. Increasing the droplet diameter causes a higher relative difference between the characteristic lengths.

Table 6 summarizes the equilibrium state parameters for the three cases considered. The non-reacting flow with adiabatic and non-evaporating droplets has the lowest pressure and density and the highest temperature and velocity. For the two other cases, the equilibrium states are close, because the small liquid mass fraction and the high molecular mass of JP-10 limit the volumetric effect of the phase transformation. Droplet evaporation results in slightly lower pressure and temperature, but higher density and velocity.

DOI: 10.13009/EUCASS2025-377

Table 5: Characteristic lengths for momentum, thermal, and mass exchange for a non-reacting flow with evaporating droplets

	D_p = 5 µm	D_p = 50 µm
l_v (m)	5.734×10^{-4}	5.717×10^{-3}
l_T (m)	9.987×10^{-4}	3.041×10^{-2}
l_m (m)	3.807×10^{-3}	1.475×10^{-1}

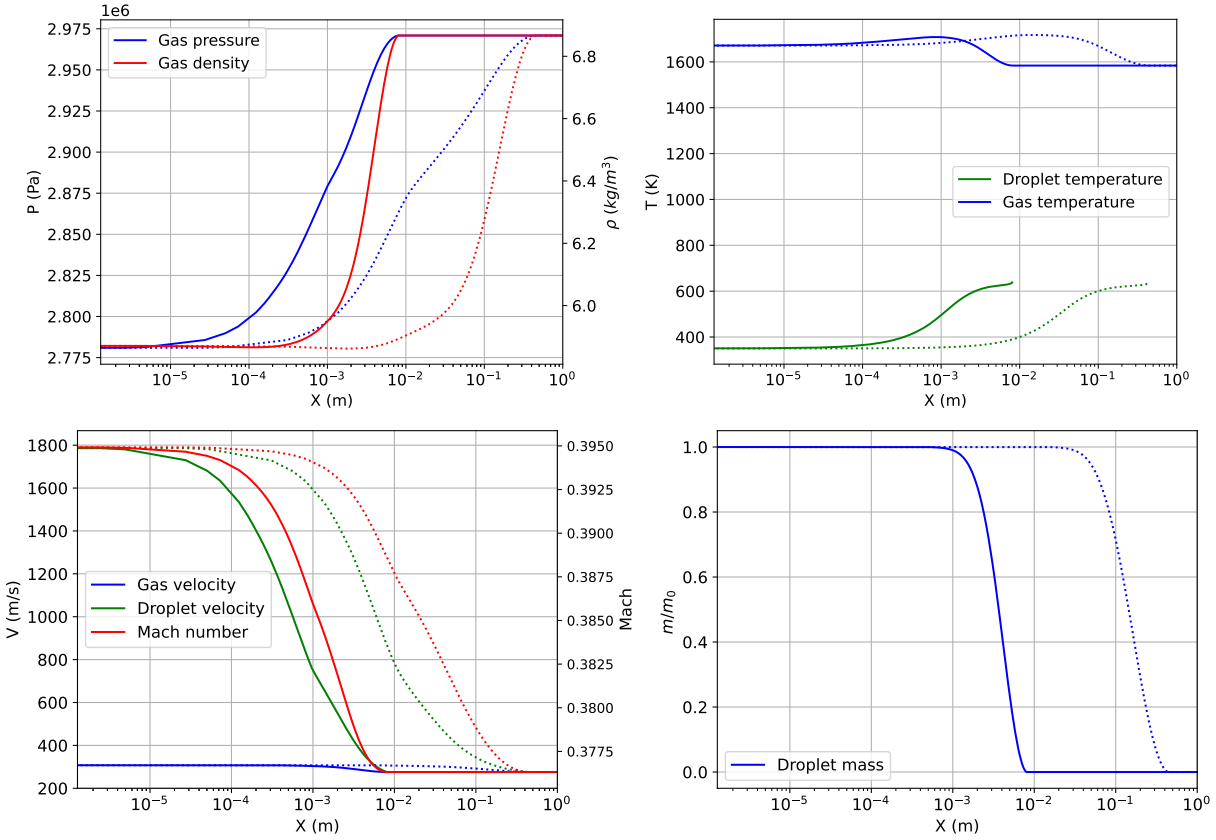

Figure 3: Parameter profiles versus post-shock distance for a non-reacting flow with evaporating droplets of 5 µm (solid lines) and 50 µm (dotted lines)

Table 6: Equilibrium state for non-reacting flow with adiabatic and non evaporating droplets (case 1), with non-evaporating droplets (case 2), and evaporating droplets (case 3)

Case	1	2	3
P_g (MPa)	2.918	2.977	2.971
T_g (K)	1730	1585	1584
ρ_g (kg/m^3)	5.951	6.628	6.867
V_g (m/s)	303.5	272.5	275.8

DOI: 10.13009/EUCASS2025-377

3.4 Detonation

Chemical reactions are activated to obtain detonation profiles shown in figure 4 for droplet diameters of 5 μm and 50 μm with 70% of the total kerosene mass in liquid phase. The initial state parameters are specified in table 2.

The initial parameter variations are quite similar to those in the previous case of evaporating droplets (figure 3) due to the ignition delay of the gaseous kerosene-air mixture. Consumption of gaseous kerosene by chemical reactions has a noticeable effect at a distance x > 0.1 mm. In particular, the heat release results in a continuous decrease in gas density and increase in gas velocity for both droplet diameters. Combustion of prevaporized kerosene (30% of the total fuel mass) ends at a distance of 2 to 4 mm and induces a first stage of pressure drop and gas temperature growth. The following stages depend strongly on the droplet size.

For D_p = 5 μm, droplet evaporation takes place on a distance from 1 to 10 mm, so it starts before the prevaporized kerosene is fully depleted. This process supports combustion continuously until the fuel is completely consumed. Therefore, the profiles of pressure, density, and temperature show monotonic variation.

For D_p = 50 μm, droplet evaporation begins at around 2 cm, being retarded by the slow droplet heating. As the prevaporized kerosene is already consumed, the combustion process is suppressed so that the profiles of pressure, density, and gas temperature show a distinct plateau before the second combustion stage.

The droplet velocity exhibits a non-monotonic behavior during the evaporation and second combustion stage. As the combustion causes a quick increase in gas velocity, the droplet velocity cannot reach equilibrium and becomes lower than the gas one after the crossing point.

The role of the physical processes within a detonation wave can be better understood by considering the profiles of global thermicity and its components displayed in figure 5. The major effect is produced by chemical reactions (σ_4). For D_p = 5 μm, the main thermicity peak is observed during the liquid kerosene consumption. For D_p = 50 μm, it is due to the prevaporized kerosene combustion, whereas the liquid fuel combustion results in a much less intense heat release, limited by the evaporation process. The components due to the momentum (σ_2) and thermal (σ_3) exchanges play an important role during a short initial period. The evaporation component (σ_5) becomes important during later stages, and is partially compensated by the mass exchange component (σ_1). The thermicity profiles exhibit a singularity at the crossing point of the gas and droplet velocities (0.004 m for D_p = 5 μm and 0.15 m for D_p = 50 μm) (figure 4). This fact indicates the importance of the convective terms in the thermal exchange and evaporation model.

The characteristic lengths evaluated for the reacting flow are summarized in Table 7. With respect to the non-reacting flow (table 5), the momentum lengths are more than twice shorter, mainly because of smaller range of velocity variation. The thermal lengths are reduced due to gas heating by combustion, but to a lesser extent. In spite of the gas heating and kerosene vapor depletion by combustion, the evaporation lengths are increased. The sole cause of this effect is the weakening of convective factors because of the rapid growth of gas velocity. The length of 50% fuel consumption is shorter than the evaporation length because only 30% of liquid fuel needs to be consumed after burning the prevaporized kerosene. The entire process of fuel consumption is almost threefold longer than the 50% consumption, as it is fully dependent on the droplet evaporation. The scales difference increases with the droplet diameter.

Table 7: Characteristic lengths for detonation

	D_p = 5 μm	D_p = 50 μm
l_v (m)	2.179×10^{-4}	2.732×10^{-3}
l_T (m)	9.107×10^{-4}	2.431×10^{-2}
l_m (m)	4.542×10^{-3}	2.119×10^{-1}
$l_{F_{0.5}}$ (m)	3.285×10^{-3}	1.162×10^{-1}
$l_{F_{0.95}}$ (m)	8.006×10^{-3}	3.547×10^{-1}

DOI: 10.13009/EUCASS2025-377

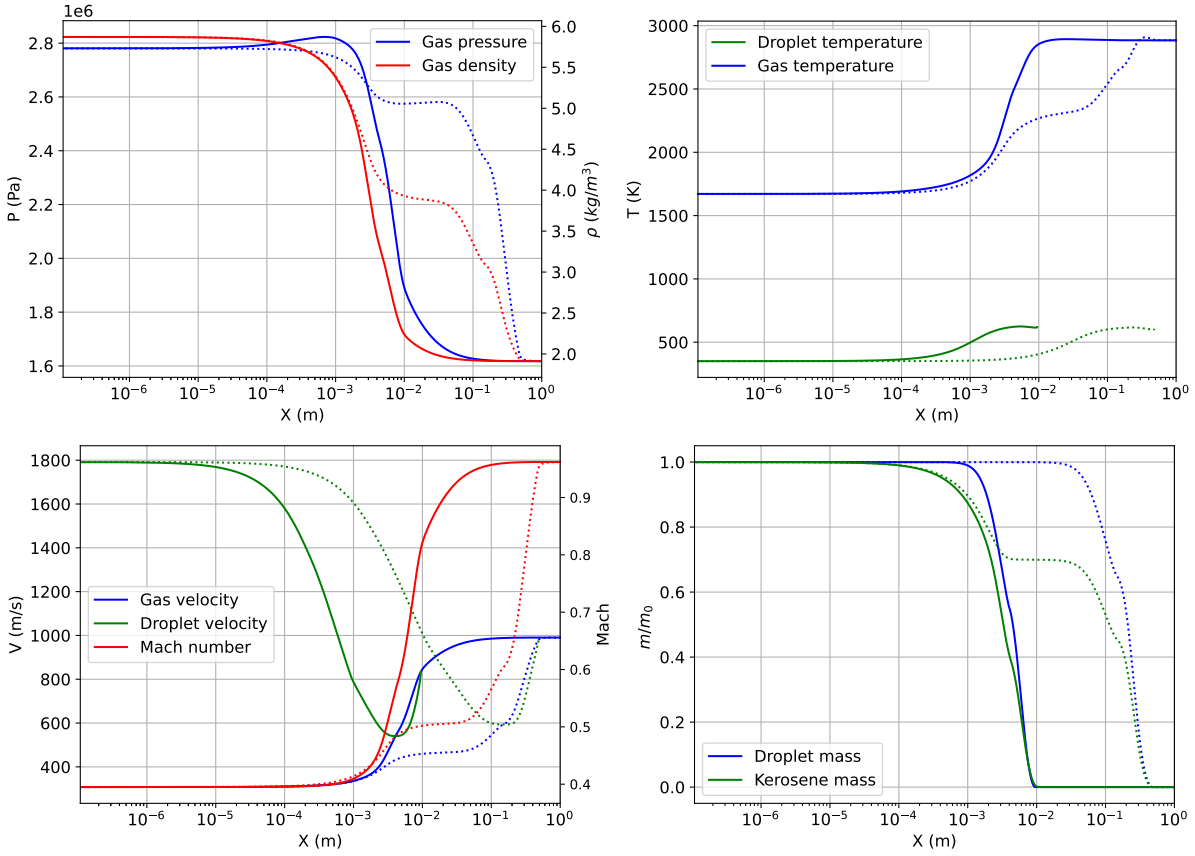

Figure 4: Parameter profiles versus post-shock distance for a detonation with droplets of 5 µm (solid lines) and 50 µm (dotted lines)

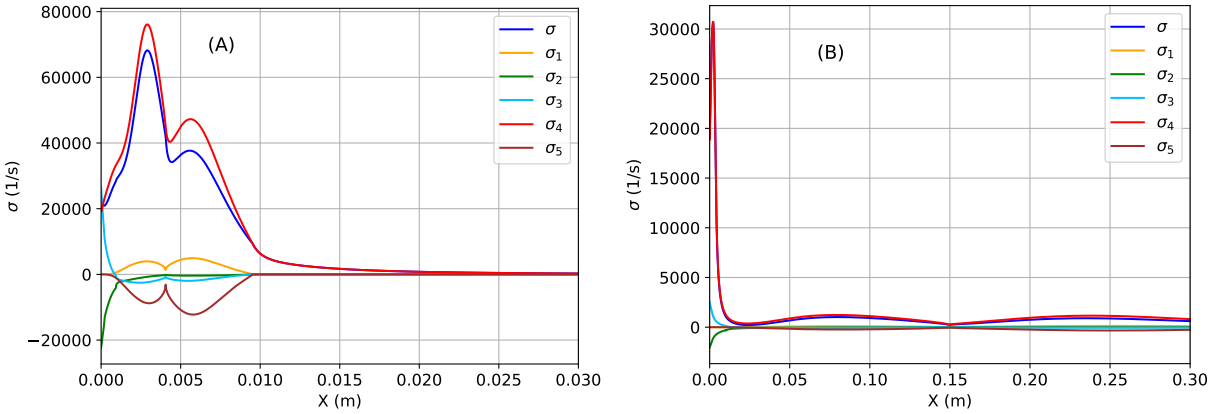

Figure 5: Profiles of global thermicity and its components versus post-shock distance for a detonation with droplets of 5 µm (A) and 50 µm (B)

Another parameter that influences detonation characteristics is the liquid mass ratio, β, defined as the liquid fraction of the full fuel mass. This ratio influences parameter profiles and characteristic lengths but also the post-shock state. Indeed, its change affects the initial thermodynamic properties of the gas phase as well as the exchange factors past the shock. Table 8 shows wave velocity values for different liquid mass ratios. As this ratio increases, the detonation velocity slightly decreases.

Figure 6 shows gas parameter profiles for detonation with droplets of 5 µm and various liquid mass ratios. Increasing the liquid mass ratio, reduces pressure and density, and increases temperature and velocity of the post-shock state. At higher β values, the pressure and density profiles exhibit a local maximum due to the particle drag effect. The

DOI: 10.13009/EUCASS2025-377

combustion process starts later, but its overall duration depends on β in a limited range < 0.5. The final state is weakly affected by β.

Figure 7 presents detonation characteristic lengths versus liquid mass ratio for droplet diameters ranging from 1 to 50 µm. The momentum, thermal, and evaporation lengths manifest a strong increasing trend with droplet diameter. In all the cases, the momentum length is the shortest, whereas the evaporation length is the largest and most sensible to diameter change. The dependence of these three characteristic lengths on the liquid mass ratio is rather weak and exhibits a positive tendency for the momentum and thermal lengths, contrary to the evaporation length, which tends to decrease. The only exception is the momentum length for the largest diameter, for which the decreasing trend can be explained by the superposition of drag force and heat release effects on the gas and droplet velocities.

The length of 50% fuel consumption increases linearly with liquid mass ratio for small droplet diameters up to 5 µm. For larger diameters, this length is strongly dependent on the liquid mass ratio within the range of 0.3 to 0.7; at a low β value, it is fully defined by combustion of the prevaporized kerosene; when β is high, the heat release from this first combustion stage has a weak effect on droplet heating and evaporation. This different behavior can be explained by separation of the combustion stages consuming prevaporized and liquid kerosene.

The length of 95% fuel consumption strongly increases with droplet diameter. For very small droplets of 1 and 3 µm, this length also shows a positive trend with liquid mass ratio. For larger droplet diameters, it has a maximum that shifts towards $\beta \approx 0.3$ as the droplet size increases. There are two factors defining this maximum: (i) the first combustion stage should produce an important heat release to increase the gas velocity so that the convective factors are quickly reduced; (ii) droplets should preserve a high velocity and travel a greater distance.

Table 8: CJ detonation velocity for various liquid mass ratios

β	0	0.1	0.3	0.5	0.7	0.9	1
D_{CJ} (m/s)	1793.4	1793.2	1792.7	1792.3	1791.8	1791.4	1791.2

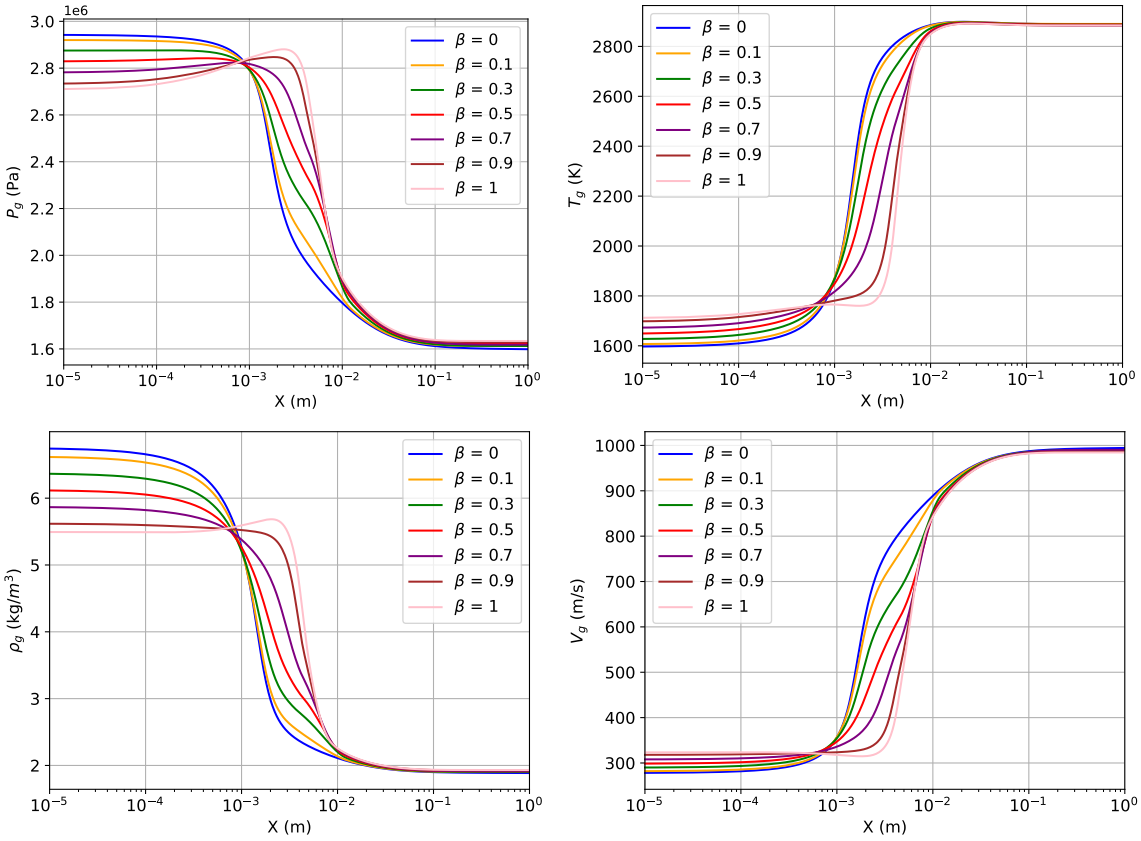

Figure 6: Gas parameter profiles versus post-shock distance for detonation with droplets of 5 µm and various liquid mass ratios

DOI: 10.13009/EUCASS2025-377

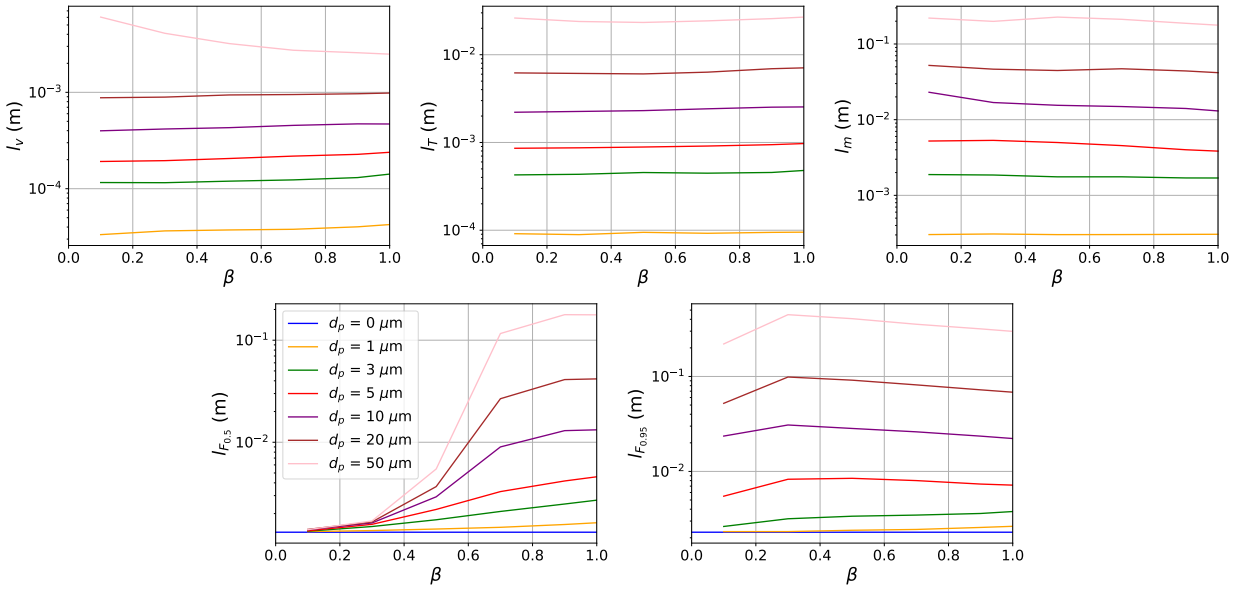

Figure 7: Characteristic lengths of detonation versus liquid mass ratio for various droplets diameters

The obtained results show that all the characteristic lengths depend strongly on the droplet diameter. The present ZND model describes an ideal case, for which this dependence has no effect on the detonation velocity or the final CJ state. When applied to a rotating detonation combustor, this dependence becomes crucial. One of the critical factors is the rarefaction wave following the detonation and producing a rapid acceleration of the combustion products to a supersonic speed with respect to the detonation front. In this case, a sonic condition can be obtained even if some fuel remains unburnt. Hence, the detonation wave intensity may be reduced due to incomplete heat release. In the worst case, only prevaporized kerosene will be burnt by detonation, and the liquid droplets will be consumed after some expansion. For this worst case, figure 8 displays plots of CJ detonation velocity versus liquid mass ratio for two droplet diameters. A decrease in the wave velocity will result in a significant reduction in the post-shock pressure and temperature, and by consequence, in an important growth of the induction length for prevaporised kerosene. This will result in a global reduction of engine thermal efficiency. Another critical factor is related to detonation stability issues due to slow combustion of the two-phase mixture. Taking into account size limitations applicable to a real combustor, detonation instability could be a major limitation to the practical use of a kerosene-fueled RDE. Both of these factors have already been reported in the literature by experimental and numerical results demonstrating detonation velocity deficit or unstable propagation.[22–24]

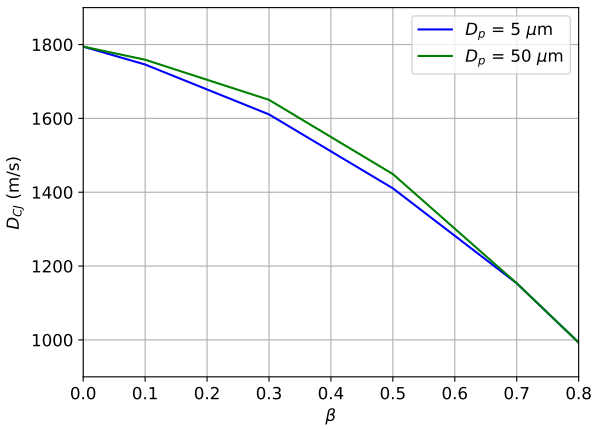

Figure 8: CJ detonation velocity versus liquid mass ratio for different droplet diameters assuming no liquid kerosene evaporation

DOI: 10.13009/EUCASS2025-377

The present study considers an ideal mixture with monodispersed droplets. In a real situation, the dispersed phase is represented by a particle size distribution. Small particles can be rapidly burnt and maintain the combustion process while larger particles are heated. On the other hand, large particles can be broken by shear forces after crossing the shock wave. One of the factors not yet taken into account in the present model is the diffusion regime of droplet combustion, which can be important for large droplets. As an example, in the evaporation model used by Hayashi et al.,[1] a reaction heat term is introduced in the Spalding number formulation. Another factor to take into account is the flow turbulence, which can influence droplet heat exchange and evaporation.

4. Conclusion

A numerical study based on ZND modeling of a detonation in a two-phase kerosene-air mixture is presented. An Eulerian-Eulerian formulation is described for a one-dimensional steady-state two-phase reacting flow behind a normal shock with physical models adapted for high-Reynolds number, compressibility and evaporation film effects.

Different physical factors (momentum, thermal and mass exchanges) are studied for non-reacting flow. Momentum exchange does not increase the gas speed but has a compression effect with an overall increase in pressure, density, and temperature. Adding thermal exchange enhances the overall variation of pressure, density and velocity. This exchange is strongly delayed compared to the momentum exchange. Mass exchange does not change the overall parameter variations, except for droplet temperature, whose growth is limited by evaporation. Droplet evaporation reduces all the characteristic lengths and becomes the slowest process. In all cases, increasing the droplet diameter causes a higher difference in the characteristic lengths.

In a reactive case, the flow structure depends on the liquid mass ratio and droplet diameter. With small droplets, the combustion process is continuous from the ignition to complete fuel consumption, whereas, with large droplets, it can be suppressed between the consumption of gaseous and liquid kerosene. An analysis of thermicity terms is presented to better understand the role of main physical factors controlling the flow behavior.

Droplet diameter has a strong effect on the characteristic lengths, causing their increase. Liquid mass ratio has lesser influence on the characteristic lengths, but contrary to droplet diameter, it affects the post-shock state mainly via gas properties and to a lesser extent by slightly decreasing detonation propagation velocity. The final CJ conditions are weakly dependent on the liquid mass ratio.

The present ZND model is an ideal case assuming monodispersed droplets, no breakup process, no flow turbulence, and no trailing rarefaction wave. However, it permits a good understanding of the processes behind a shock in a two-phase reacting mixture. It can be exploited to perform parametric studies by varying the initial conditions (equivalence ratio, temperature, pressure,...), to test different physical models, and to have a reference solution for more complex 2D or 3D cases.

5. Acknowledgments

This study was funded by the General Scientific Direction of ONERA and the Scientific Direction of DSO.

References

[1] A. K. Hayashi, N. Tsuboi, and E. Dzieminska. Numerical study on JP-10/air detonation and rotating detonation engine. *AIAA Journal*, 58(12):5078–5094, 2020.

[2] X. Han, Y. Huang, Q. Zheng, Qiang X., Han X., Fang W., Yuwen W., Wenkang F., and Chunsheng W. Study of the characteristics and combustion efficiency of liquid kerosene/oxygen-enriched air rotating detonation wave with different modes. *Fuel*, 355:129424, 2024.

[3] B. J. Musick, M. Paudel, P. K. Ramaprabhu, and J. A. McFarland. Numerical simulations of droplet evaporation and breakup effects on heterogeneous detonations. *Combustion and Flame*, 257:113035, 2023.

[4] C. J. Young, V. O. Duke-Walker, and J. A. McFarland. Droplet breakup and evaporation in liquid-fueled detonations. *Experimental Thermal and Fluid Science*, 160:111324, 2025.

[5] J.M. Powers, D.S. Stewart, and H. Krier. Theory of two-phase detonation — part i: Modeling. *Combustion and Flame*, 80(3):264–279, 1990.

[6] J.M. Powers, D.S. Stewart, and H. Krier. Theory of two-phase detonation — part ii: Structure. *Combustion and Flame*, 80(3):280–303, 1990.

DOI: 10.13009/EUCASS2025-377

[7] F. Zhang, K. Gerrard, and R. C. Ripley. Reaction mechanism of aluminum-particle-air detonation. *Journal of Propulsion and Power*, 25(4):845–858, 2009.

[8] Q. Zhou, J. Huang, W. Han, and C. Wang. Initiation and propagation of one-dimensional detonations in aluminum-particle/C2H2/air system. *Physics of Fluids*, 34(12):126109, 12 2022.

[9] D. Martínez-Ruiz. On the structure of steady one-dimensional liquid-fueled detonations. *Physics of Fluids*, 35(8):086122, 08 2023.

[10] F. Zhang. In Shock wave science and technologiy reference library. *Springer*, 4:148–149, 2009.

[11] B. Varatharajan, M. Petrova, F. A. Williams, and V. Tangirala. Two-step chemical-kinetic descriptions for hydrocarbon-oxygen-diluent ignition and detonation applications. *Proceedings of the Combustion Institute*, 30(2):1869–1877, 2005.

[12] L. Schiller and A. Naumann. A drag coefficient correlation. *Zeitschrift des Vereins Deutscher Ingenieure*, 77:318–320, 1935.

[13] C. B. Henderson. Drag coefficients of spheres in continuum and rarefied flows. *AIAA Journal*, 14(6):707–708, 1976.

[14] E. Loth. Compressibility and rarefaction effects on drag of a spherical particle. *AIAA Journal*, 46(9):2219–2228, 2008.

[15] B. Abramzon and W. A. Sirignano. Droplet vaporization model for spray combustion calculations. *International Journal of Heat and Mass Transfer*, 32(9):1605–1618, 1989.

[16] M. Yuen and Longfei Chen. On drag of evaporating liquid droplets. *Combustion Science and Technology*, 14:147–154, 1976.

[17] W. Ranz and W. Marshall. Evaporation from drops. *Chemical Engineering Progress*, 48(4):141–146, 1952.

[18] D. J. Carlson and R. F. Hoglund. Particle drag and heat transfer in rocket nozzles. *AIAA Journal*, 2(11):1980–1984, 1964.

[19] A. C. Hindmarsh. Odepack, a systemized collection of ode solvers. *Scientific computing*, 1983.

[20] L. Petzold. Automatic selection of methods for solving stiff and nonstiff systems of ordinary differential equations. *SIAM Journal on Scientific and Statistical Computing*, 4(1):136–148, 1983.

[21] EDL. SDToolbox: Numerical Tools for Shock and Detonation Wave Modeling. GALCIT Report FM2018.001, Pasadena, CA, Apr 2023.

[22] M. Zhao and H. Zhang. Rotating detonative combustion in partially pre-vaporized dilute n-heptane sprays: Droplet size and equivalence ratio effects. *Fuel*, 304:121481, 2021.

[23] Zhaoxin R. and Longxi Z. Numerical study on rotating detonation stability in two-phase kerosene-air mixture. *Combustion and Flame*, 231:111484, 2021.

[24] Q. Zheng, H. Meng, C. Weng, Y. Wu, W. Feng, and M. Wu. Experimental research on the instability propagation characteristics of liquid kerosene rotating detonation wave. *Defence Technology*, 16(6):1106–1115, 2020.